RSC Advances

ROYAL SOCIETY OF CHEMISTRY

www.rsc.org/advances

Single-step synthesis of Carbon Nanotubes/Iron/Iron oxide composite films through inert-ambient CVD using ferric acetylacetonate as precursor

Pallavi Arod[a] and S.A. Shivashankar[a,b*]

[a]*Materials Research Centre,* [b]*Centre for Nano Science and Engineering, Indian Institute of Science, Bangalore-560012, India*

Graphical abstract

Iron, iron oxide (Fe_3O_4)-carbon nanotube(CNT) composite thin film was obtained by single step chemical vapor deposition(CVD) process using $Fe(acac)_3$ as the sole precursor. Depending on the deposition parameters employed the carbon content in the film can be amorphous carbon or CNT.

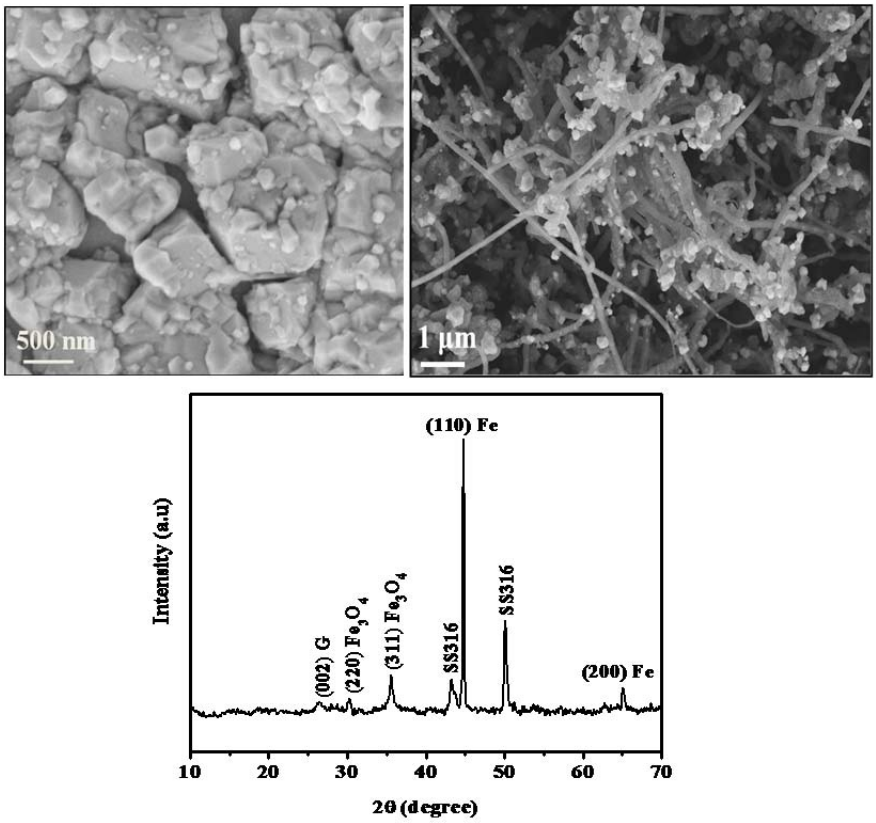

* Corresponding author. Tel: +91 80 2293 3323. Email address: shivu@cense.iisc.ernet.in (S.A. Shivashankar)

Single-step synthesis of Carbon Nanotubes/Iron/Iron oxide composite films through inert-ambient CVD using ferric acetylacetonate as precursor

Pallavi Arod[a] and S.A. Shivashankar[a,b*]

[a]*Materials Research Centre,* [b]*Centre for Nano Science and Engineering, Indian Institute of Science, Bengaluru-560012, India*

Abstract

We have developed a unique single-step chemical vapor deposition (CVD) route for the synthesis of composite thin films containing carbon nanotubes (CNT). CVD was carried out in inert ambient using only iron (III) acetylacetonate as the precursor. Depositions were conducted at 700°C on stainless steel substrates in argon ambient in the absence of any reactive gases (such as oxygen, hydrogen). By changing deposition parameters, especially the pressure in the CVD reactor, the form of carbon deposited could be changed from amorphous to carbon nanotubes, the latter resulting in Fe-Fe_3O_4-CNT films. X-ray diffraction, Raman spectroscopy, X-ray photoelectron spectroscopy, and electron microscopy together confirm the formation of the three-component composite and illustrate the nanoscale mixing of the components. Elemental iron formed in this process was protected from oxidation by the co-deposited carbon surrounding it. Irrespective of the substrate used, a composite coating with CNTs was formed under optimum conditions, as verified by analyses of the film formed on polycrystalline alumina and silicon substrates.

Introduction

Metal oxide-carbon composites offer the opportunity to explore their potentially superior material characteristics relative to the constituents, as the properties of individual components can result in a synergetic effect when they are parts of a composite. The many desirable attributes of carbon - such as its mechanical strength, stiffness, electrical conductivity, ready availability, cost-effectiveness, low density, chemical stability, and amenability to processing for tailoring its form and properties - make "carbons" sought-after candidates in composite formation. Composites of metals, metal oxide with various forms of carbon such as nanotubes,

* Corresponding author. Tel: +91 80 2293 3323. Email address: shivu@cense.iisc.ernet.in (S.A. Shivashankar)

fibers, spheres, aerogel, graphene etc., have been prepared and studied for their applications in sensors, catalysis, energy storage devices and structural materials, giving rise to improved functional materials [1-8]. In particular, carbon nanotubes (CNT) and their composites have been the subject of much worldwide research and development (R&D) effort over the last two decades [5, 7, 9-11].

Most of the reported methods for preparing CNT-metal oxide composites are multi-step processes using distinct starting materials (precursors) as sources for carbon and the metal oxide. Solution-based methods involve separate synthesis of CNTs, followed by adding them to the solution containing the precursor to the metal oxide. From this solution, the metal oxide is obtained through the sol-gel method, chemical precipitation, impregnation, solvothermal methods or electrodeposition, in the presence of CNTs, thus forming a composite[2, 9, 12-17]. The primarily two-step procedure may include an additional step where CNTs are acid-treated for better dispersion in the solution[15, 18].

Thin films of metal oxide/CNT composites are usually obtained through distinct deposition steps in a preset sequence using appropriate starting materials for each of the constituents. Typically, CNTs are obtained by chemical vapor deposition (CVD) and the oxide phase deposited by sputtering, CVD or electrodeposition[16, 19-22]. In contrast with the aforementioned methods, our approach has been to use a metalorganic compound (in this case ferric acetylacetonate), which contains direct Fe-O bonds as well as hydrocarbon groups in its molecular structure, as precursor in CVD and to arrive at the deposition conditions needed to obtain metal oxide-CNT composite thin films.

The present effort was prompted by the results obtained earlier in the author's research group on MnO/C composites obtained by a similar inert-ambient CVD process employing manganese acetylacetoante as precursor. The MnO/C coatings on stainless steel proved to be excellent electrodes for thin film supercapacitors[23]. Magnetic measurements made on such coatings (on alumina substrate) have been reported[24]. Our work on inert-ambient CVD using $Fe(acac)_3$ was initiated with the expectation that similarly excellent (thin film) electrode materials can be obtained. What we obtained instead were the three-component C/Fe/Fe_3O_4 composites reported here.

Iron exists in +3 and +2 oxidation states, forming several distinct oxide phases, of which α-Fe_2O_3 is the most stable. Fe_3O_4 and γ-Fe_2O_3 are technologically important due to their

magnetic ordering, the latter finding applications in magnetic recording media [25-27]. Even though iron oxides are very well known materials, they are today being explored in their nanometric form for their magnetic, catalytic, sensing, and energy storage properties [27-30]. Nanoparticles of iron oxides and their nanostructured thin films have been prepared by various chemical methods. In particular, CVD of iron oxide films has been carried out in flowing oxygen, using solid precursors such as ferric acetylacetonate [$Fe(acac)_3$] or iron carbonyl [$Fe(CO)_5$], with argon as the carrier gas, typically in the temperature range of 350-550^oC [31-34]. Careful control of the oxygen partial pressure and substrate temperature is required in such a process to obtain Fe_3O_4 or the metastable phase γ-Fe_2O_3 (rather than α-Fe_2O_3). Furthermore, CVD is widely employed to obtain CNTs, using various hydrocarbons, alcohols, and organometallics, such as metallocenes of Fe, Ni and Co, as precursor [35-38].

We report here on a single-step process for the formation of a thin film composite of CNTs, iron, and iron oxide by CVD. This method uses a metalorganic complex of iron as the single-source precursor, which contains both iron-oxygen bonds and hydrocarbon moieties in its molecular structure. Specifically, the CVD process was carried out in an inert ambient using ferric acetylacetonate as the precursor. Under certain deposition conditions, in the absence of any reactive gas such as O_2, H_2, etc., a three-component composite film consisting of elemental iron, Fe_3O_4, and carbon nanotube is obtained. By "tuning" the deposition conditions, the nature of the carbon in the composite can be varied from amorphous carbon to CNTs. We have recently provided a brief report rationalising the formation of Fe/Fe_3O_4/carbon composites through equilibrium thermodynamic modeling of the inert-ambient CVD process[39].

It is relevant to note here that C/Fe/Fe_3O_4 camposites, including those with carbon in the form of CNTs, have been studied by various investigators, with different applications in mind. These include: as anode material in lithium-ion batteries[40, 41]; in waste water treatment[42]; in catalysis and the abatement of the environmental hazards[43, 44].

Experimental

The molecular structure of the precursor, ferric acetylacetonate, $Fe(acac)_3$, is shown in the inset of Fig.1. The complex is a crystalline solid that sublimes above ~140°C. Fig.1 shows data from the simultaneous thermogravimetry (TG) and differential thermal analysis (DTA) of $Fe(acac)_3$ (obtained from a SDT Q600 TG/DT Analyzer, TA Instruments, USA). TG data show that, as temperature is raised, a modest weight loss begins at about 125°C. Much of the weight loss occurs in a single step monotonic loss in weight as the temperature is raised. Weight loss occurs in a single step spanning ~170-220°C, leaving a substantial residue. The shaded area in the TGA graph indicates the range of temperatures, ~150-160°C, at which the complex may be maintained so that an adequate (and optimum) flux of the precursor vapor is available during the CVD process. Over this range, the precursor flux would be a mild function of temperature. It is to be noted from the DTA graph that the complex melts or decomposes only at temperatures significantly higher than the vaporization temperature employed in the present work.

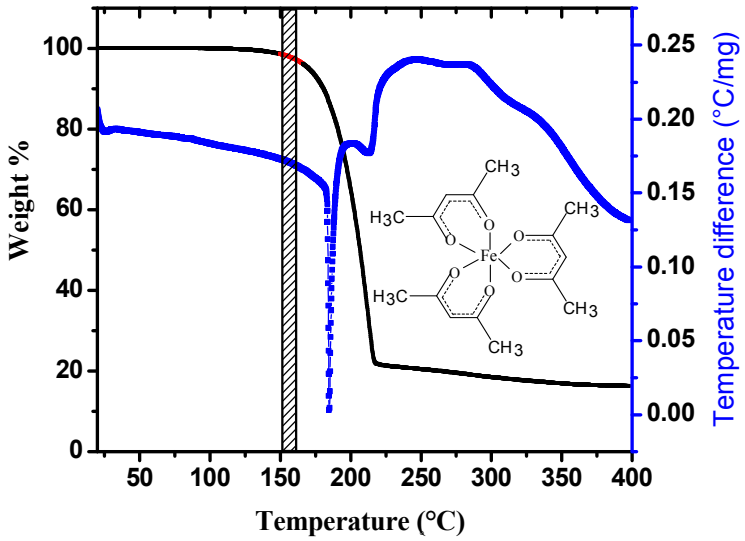

Fig.1 Simultaneous TG-DTA data for $Fe(acac)_3$ obtained under a flow of dry nitrogen, at a heating rate of 10°C/min

Depositions were carried out in a horizontal, hot-wall, low-pressure CVD reactor built in house. The reactor chamber is a fed quartz tube wherein cleaned substrates were placed. The precursor, ferric acetylacetonate (Alfa Aesar, 99.9%), was taken in a quartz boat in finely powdered form, and placed inside the vaporizer. Ultra-high purity argon served as both the carrier and purging gas. Intentionally, no reactant gas, such as oxygen or hydrogen, was used in

the CVD process. Calibrated electronic mass flow controllers (MFC, MKS-made, USA) were used for the precise control of gas flow. The CVD chamber was evacuated by a rotary pump and the pressure in the reactor is measured by a heated capacitance manometer (Baratron, MKS-made, USA) placed close to the reaction chamber. Pressure in the chamber was adjusted using a precision needle valve in line with the throttle valve. Depositions were carried out mostly on stainless steel (SS316) substrates and in some cases on single-crystalline silicon [Si(100)] and polycrystalline alumina. Depositions were conducted at 700°C, with carrier gas (argon) flow rate in the range 20-40 sccm, and the deposition pressure in the range 5-30 torr.

Characterization

X-ray diffraction (XRD) patterns of films were recorded using a PanAnalytical powder diffractometer with Cu-K_α radiation (λ=1.5418Å). Scanning electron microscopy (SEM) data were obtained in a field emission scanning electron microscope (FESEM, Zeiss Ultra55). Transmission electron microscopy (TEM) was carried out on film samples separated carefully from the substrate (TECNAI F30). X-ray photoelectron spectroscopy (XPS) was performed using Mg-K_α radiation (1253.5 eV) in a high-resolution spectrometer equipped with auto charge neutralization (AXIS ULTRA, Krotos, UK). Raman spectra were obtained using an argon ion laser of wavelength 514 nm (Horiba Jobin-Yvon LabRAM HR 100 spectrometer).

Results and Discussion

All the depositions resulted in black, adherent coatings, suggesting the presence of elemental carbon in them.

The morphology of the coating (Fig. 2(a)) obtained at 5 torr shows the aggregation of submicron-sized, faceted particles which appear to be crystalline. The coating was examined for the presence of elemental carbon by Raman spectroscopy, which is a powerful tool for affirming the presence of iron oxides as well as the different forms of carbon. The Raman spectrum of the film (Fig. 2(b)) shows peaks centered at 1340 cm^{-1} (D), 1590 cm^{-1} (G), and 2700 cm^{-1} (G′), each of which is characteristic of carbon, thus confirming the presence of elemental carbon. The G peak is characteristic of sp^2 carbon, representing the E_{2g} vibrational mode of graphitic carbon. The D peak at 1350 cm^{-1} is due to the A_{1g} lattice vibration mode of graphite, which arises only in the presence of defects, but is otherwise absent in graphite[45, 46].

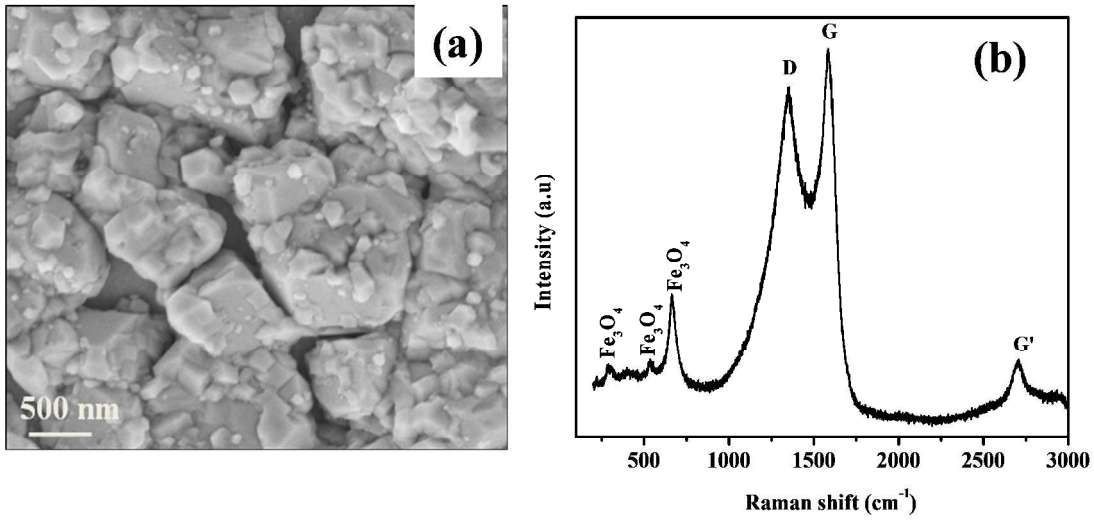

Fig. 2(a) SEM micrograph and (b) Raman spectrum of the composite film on SS316 obtained at 5 torr

The G′ band at 2700 cm^{-1} is a second order feature that appears in the presence of structural ordering, indicating a well-crystallized graphite lattice. For the present sample, this peak is of a relatively low intensity, with slight broadening. The broad and overlapping D and G peaks indicate the presence of a substantial proportion of amorphous carbon in the coating[47-49]. The Raman spectrum also features a peak at 667 cm^{-1}, which is due the A_{1g} vibrational mode of magnetite (Fe_3O_4); weaker peaks corresponding to T_{2g} vibrational mode of Fe_3O_4 are also seen, at 520 and 305 cm^{-1} [50-52]. Raman analysis therefore confirms the formation of a composite film comprising carbon and iron oxide (Fe_3O_4).

An increase in the CVD process pressure to 10 torr resulted in the formation of copious amounts of carbon nanotubes (Fig. 3(a)), with a few large particles (akin to those formed at 5 torr) underneath the CNTs (Fig. 3(b)). Correspondingly, the Raman spectrum of these coatings (Fig. 3(c)) shows sharp and strong G and G′ peaks, along with the D peak. The absence of the radial breathing mode (RBM) implies the absence of single-walled carbon nanotubes (SWCNTs), thus indicating that the CNTs formed are multi-walled carbon nanotubes (MWCNTs) [53]. The Raman spectra also feature a peak at 667 cm^{-1}, corresponding to magnetite. (To avoid the possibility of sample oxidation under laser impact during Raman analysis, laser power was kept <3 mW).

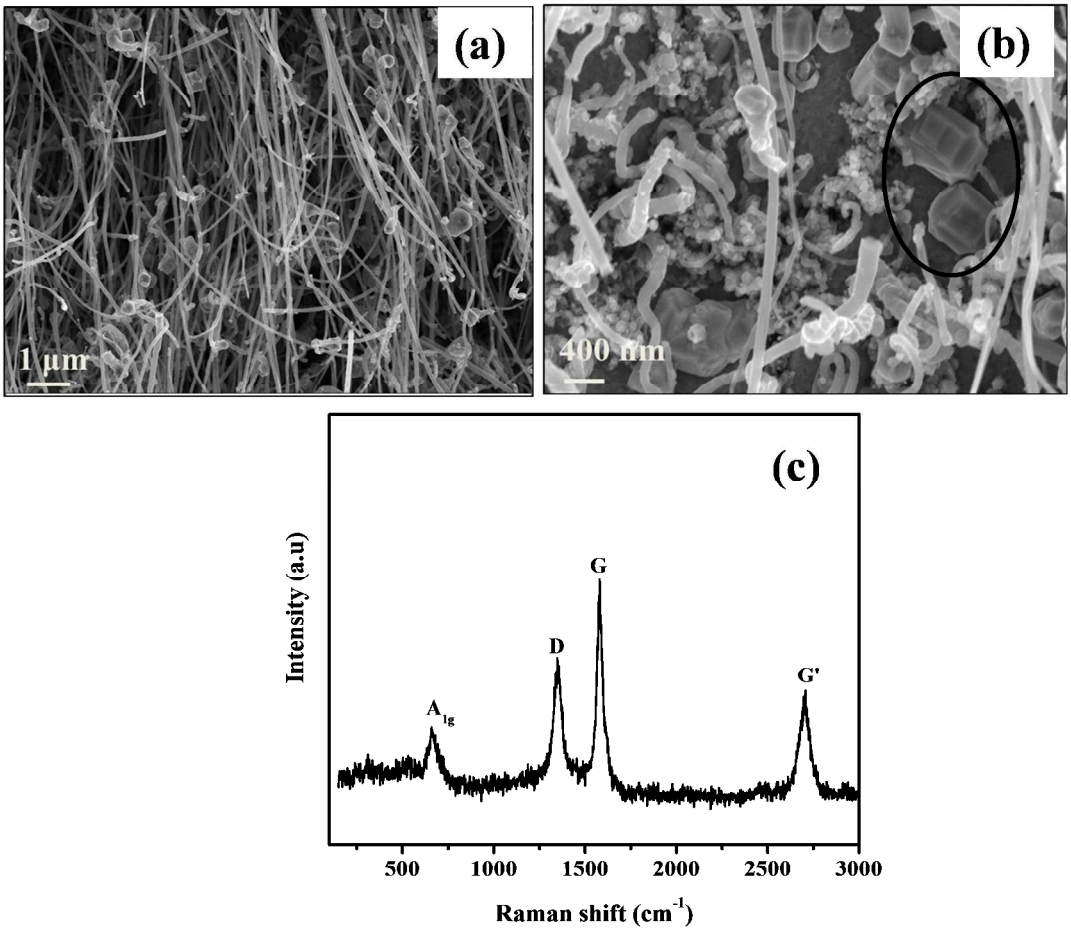

Fig. 3(a), (b) SEM micrograph of film obtained at 10 torr displaying CNTs and underlying particles (b) Raman spectrum of such a film, which confirms the presence of magnetite and CNTs

Likewise, as depositions were conducted at increasing pressures, the formation of a composite film of CNTs and iron oxide was observed upto 30 torr. The surface morphology of the composite film obtained at 30 torr and the corresponding Raman spectrum, confirming its composite character are shown Fig. 4(a) and (b). The relative intensities of the G and D peaks indicate the presence of crystalline carbon with a relatively low density of defects.

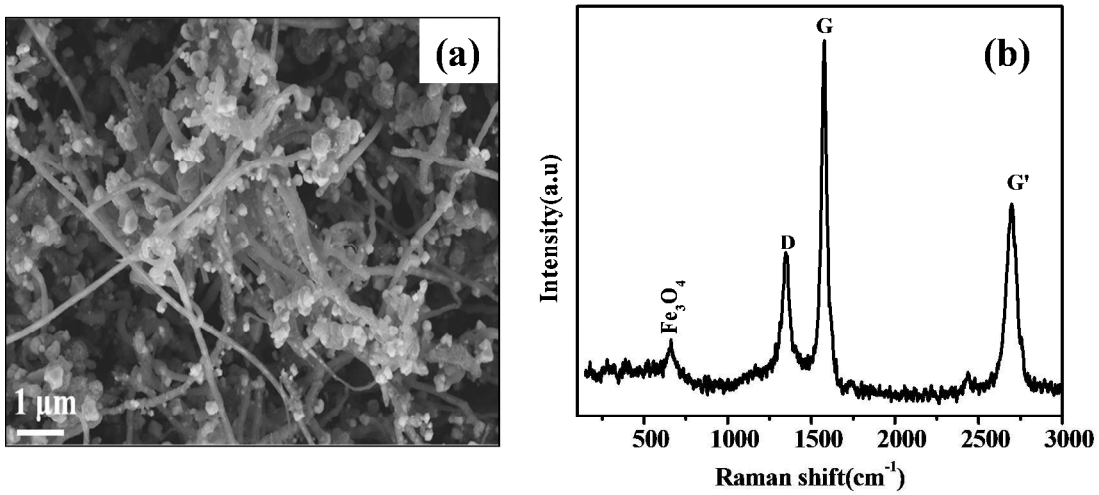

Fig. 4(a) SEM micrograph and (b) Raman spectrum of the composite film on SS316 obtained at 30 torr

These data show that, under the CVD conditions cited, the formation (deposition) of a CNT-Fe_3O_4 composite takes place through the simultaneous deposition and intergrowth of CNTs and Fe_3O_4, so that the two components are "mixed' on a very fine scale. This is reflected clearly in the SEM micrograph of the film shown in Fig. 4(a), 5(a) and in the bright-field TEM image Fig. 5(b).

The TEM micrograph (Fig. 5(b)) shows MWCNTs surrounded by particulate iron oxide. The length of CNTs formed is in the range l - 10 µm, with the diameter in the range of 80-150 nm. (Some of the CNTs may be much longer than 10 µm, though this cannot be ascertained due to the tangled nature of growth.) The CNTs obtained have well-graphitized walls and many are found to be "filled". That is, a short length of the tubes encloses a material of a high atomic number, presumably related to iron, as indicated by the TEM micrographs (Fig. 5(c)).

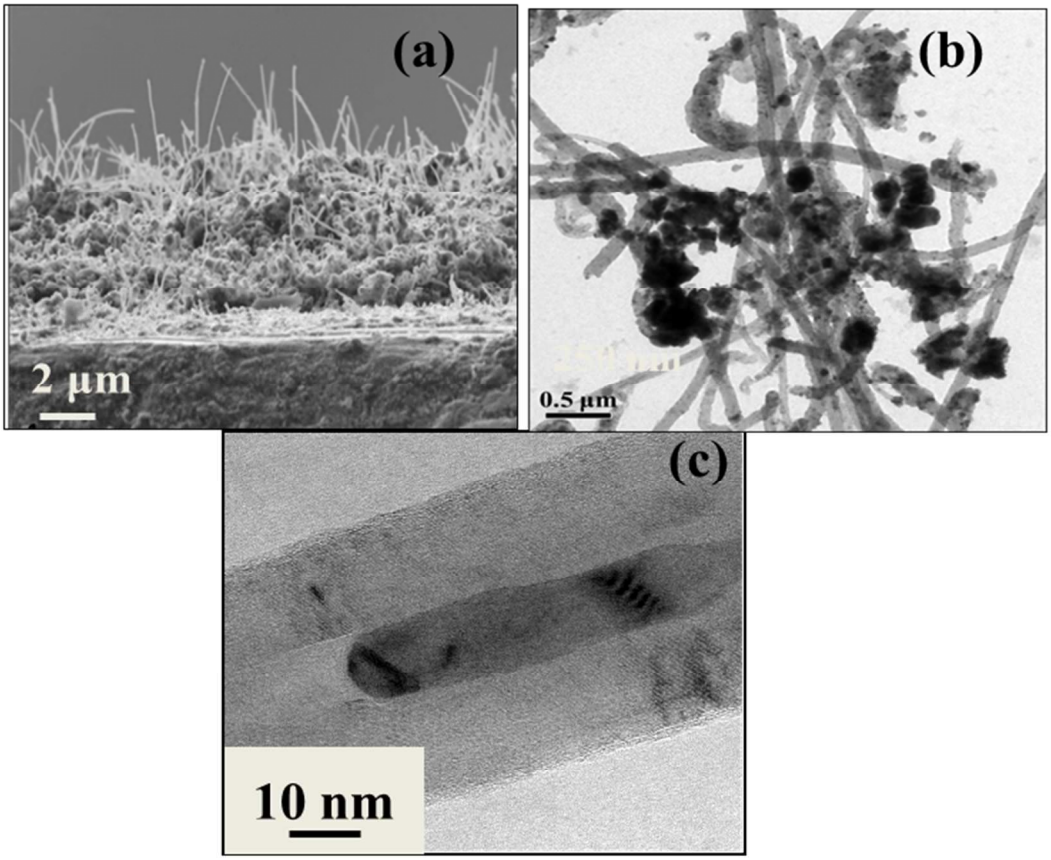

Fig. 5(a) Cross-sectional SEM of the CNT/magnetite composite deposited on SS316 @30 torr (b) TEM bright-field image of CNT/iron oxide composite with (c) showing the filled inner cavities of CNTs

Thus, inert-ambient, low-pressure CVD with the metal organic complex $Fe(acac)_3$ provides a single-step chemical process for the formation of a composite film of CNTs and iron oxide. By varying the reactor pressure, it was possible to vary the form of carbon obtained, from amorphous to crystalline CNTs.

Characterization the $Fe/Fe_3O_4/C$ composite

The composite nature of the deposits was further corroborated by XRD. Fig. 6 shows the typical XRD pattern of the coating on SS316 formed at 30 torr and 700°C. Diffraction peaks corresponding to magnetite (JCPDS file no. 19-0629) and the (002) reflection of graphite (JCPDS file no. 75-1621) were observed. Along with these two, there was a sharp peak at 44.7°, which could be due to either elemental iron or iron carbide. Similar XRD patterns were also observed on films deposited at lower pressure albeit with the absence of graphite (002) peak. Since deposition was carried out with a precursor containing hydrocarbon groups, which might

result in a carbon-rich environment at a high temperature with a stainless steel substrate present, the formation of various iron carbides could not be ruled out.

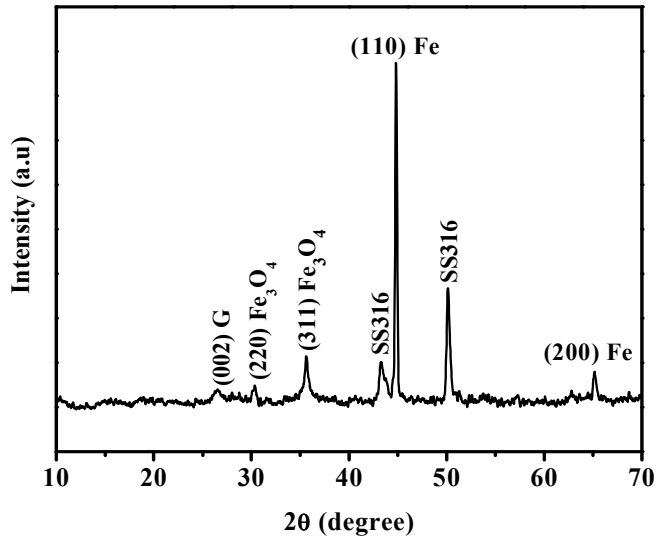

Fig. 6 XRD pattern of the composite film revealing the different constituents of the composite coating formed on SS316 at 700°C and 30 torr

Therefore, films were deposited simultaneously on alumina and SS316 substrates. The peak at 44.7°, attributable to elemental iron, is present in the XRD pattern (Fig.7) of the film grown on alumina substrate as well; this shows the formation of Fe is independent of the used.

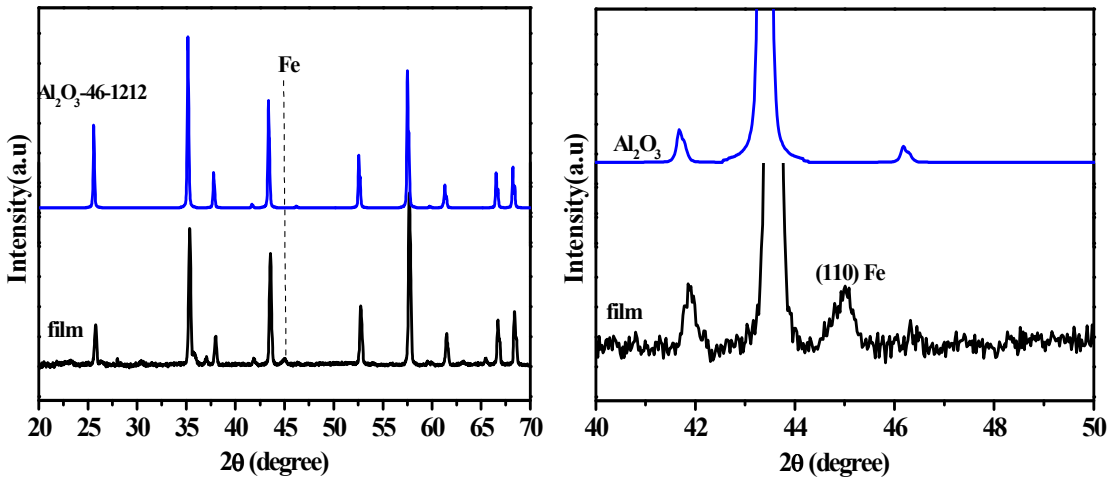

Fig. 7 Comparison of XRD patterns of alumina substrate before and after deposition at 700 °C. The standard pattern for α-Al_2O_3 is shown in blue and that of the coated substrate in black. The magnified pattern on the right shows evidence for the deposition of Fe.

XPS analysis of the composite coatings was carried out to confirm the presence of elemental iron and Fe_3O_4, The Fe 2p spectrum (Fig. 8)) consists of photoelectron peaks corresponding to both Fe^{2+} (709.5eV) and Fe^{3+} (711.1eV), whereas the Fe^{3+} satellite feature at 719 eV was absent. These data, together, confirm the presence of Fe_3O_4[54, 55].

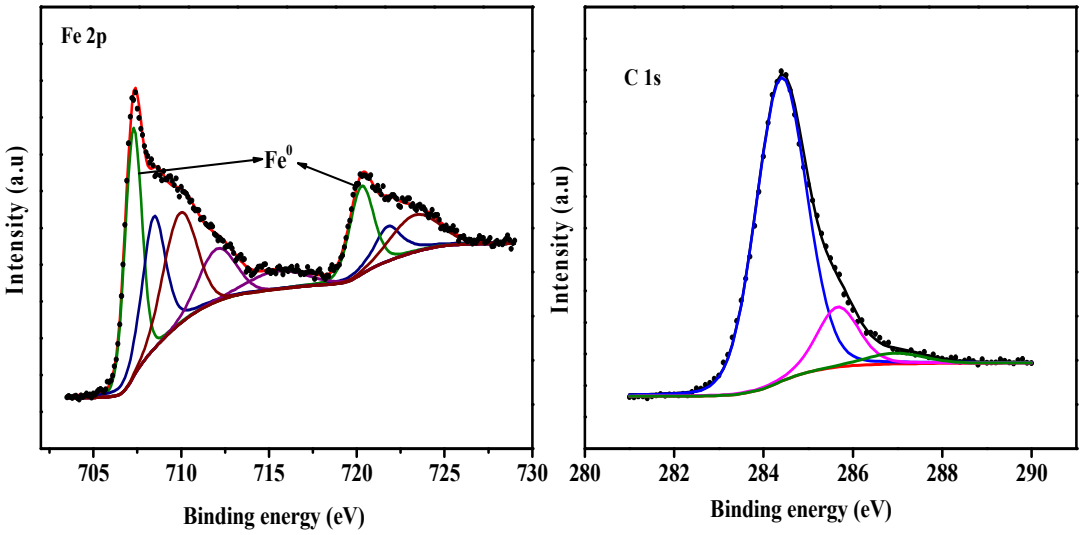

Fig. 8 Fe 2p and C 1s spectra of the coating of the coating formed on SS316 at 30 torr

A sharp photoelectron peak at 707.1 eV in the $2p_{3/2}$ spectrum, corresponding to elemental iron, could be clearly discerned[40, 54-56]. Thus, XPS data convincingly establish the presence of elemental iron in the film. Furthermore, the core level C1s spectrum does not show a peak at 283 eV, which proves the absence of iron carbide (Fig. 8).

TEM analysis was carried out to identify the constituents of the films on the nanoscale. The bright-field TEM image (Fig. 9(a)) shows relatively large (sub-micron sized) and well-faceted entities with a complex structure. The electron diffraction pattern taken on the faceted side yields a single-crystalline spot pattern corresponding to elemental iron, which is superposed on diffraction rings due to carbon and polycrystalline Fe_3O_4. This reveals convincingly the simultaneous formation and intimate coexistence of iron with iron oxide and carbon at the nanoscale.

From XRD, XPS, and TEM measurements, it is apparent that low-pressure, inert-ambient CVD using $Fe(acac)_3$ results in the formation of coatings comprising iron, iron oxide (Fe_3O_4), and carbon.

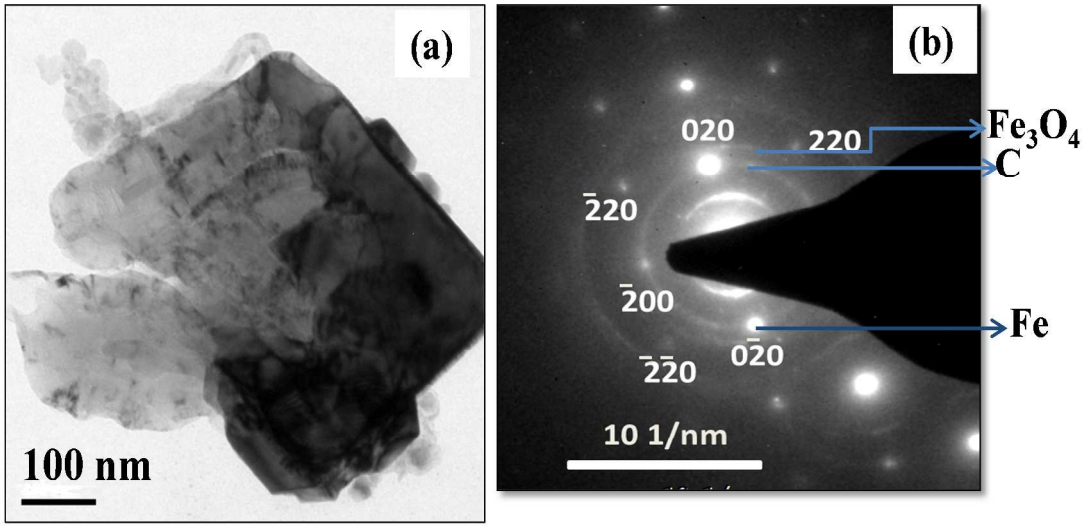

Fig. 9(a) Bright-field TEM image of a faceted particle present in the composite film formed at 10 torr (b) SAED pattern taken on particle confirms various phases which are part of single particle. Ring patterns due to iron oxide, carbon, and diffraction spots due to elemental iron could be observed (zone axis-[001])

A better understanding of the CVD growth process leading to the formation of composite coatings can be gained from TEM shown above (Fig. 9), together with a careful and detailed SEM examination of the coatings formed at different pressures in the CVD reactor. On steel substrates, the initial layers are found to be made of large (500 – 1000 nm) crystals of Fe and Fe_3O_4, along with carbon. Often, Fe and Fe_3O_4 are found to be parts of the same "grain". Carbon is deposited on these entities and surrounds them.

There is thus evidence that two processes take place -

- Formation of large (500-1000 nm) particles, which consist of Fe, Fe_3O_4, and carbon (Fig.10(a))
- Formation of CNTs, along with iron oxide nanoparticles (Fig. 10(c))

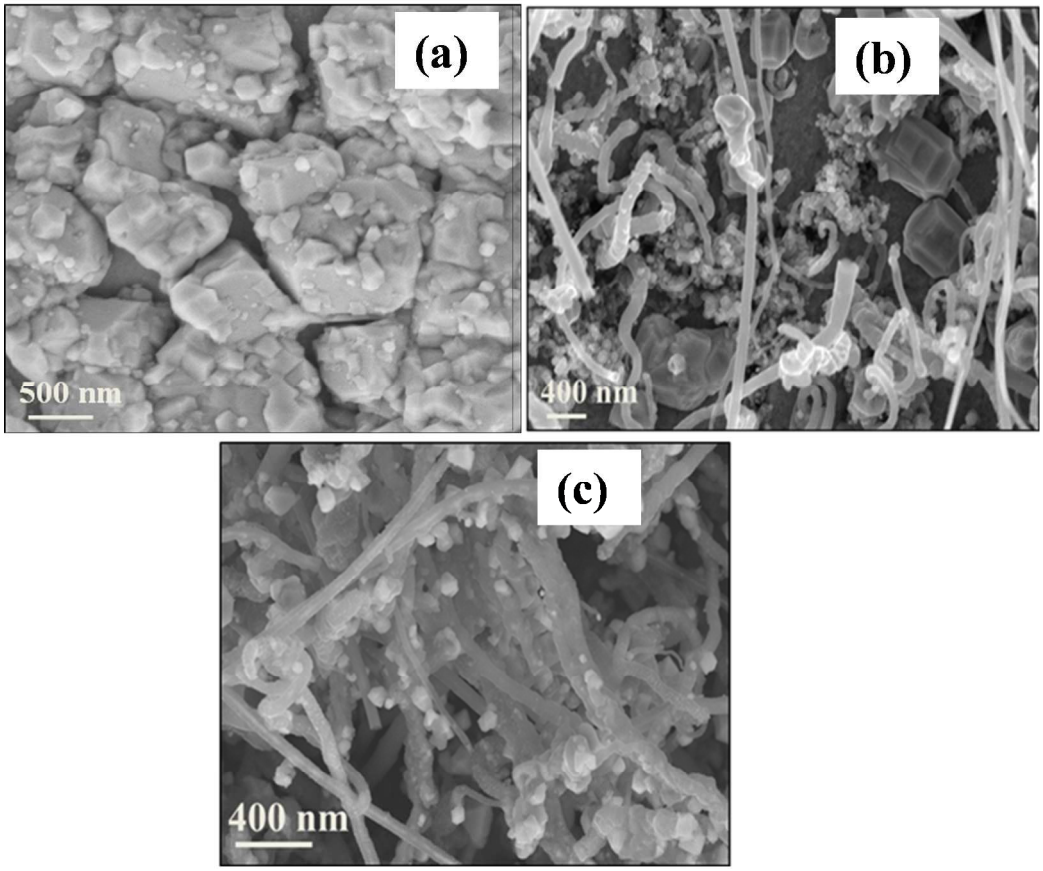

Fig. 10 An illustration of the different film morphologies obtained on SS316 under different CVD conditions, using $Fe(acac)_3$ as the precursor

The formation of large particles appears to be the first step in the formation of the deposit, which may continue, resulting in morphology shown in Fig. 10(a). Alternatively, carbon nanotube growth can take place, depending on the deposition conditions, leading to the film shown in Fig.10(c). In Fig. 10(b), there are large grains, which are few in number and are covered with tubular carbon structures. It is to be noted from Figures 9 and 10 that the crystals of elemental iron formed in the process can be rather large, perhaps as large as several hundred nm. Given the relatively large size of the particles of iron that presumably catalyse the formations of CNTs, those that are formed are expected to be multi-walled; this is evidenced by Raman analysis.

CNT growth on other substrates

As noted earlier, depositions were also conducted at 700°C *simultaneously* on SS316, Si(100), ceramic alumina (Al_2O_3) substrates, placing them side by side in the deposition

chamber. CNTs were found to form also on Si (100) and polycrystalline alumina, as shown by SEM micrograph in Fig.11 and further confirmed by Raman spectroscopy (Fig. 11(c)).

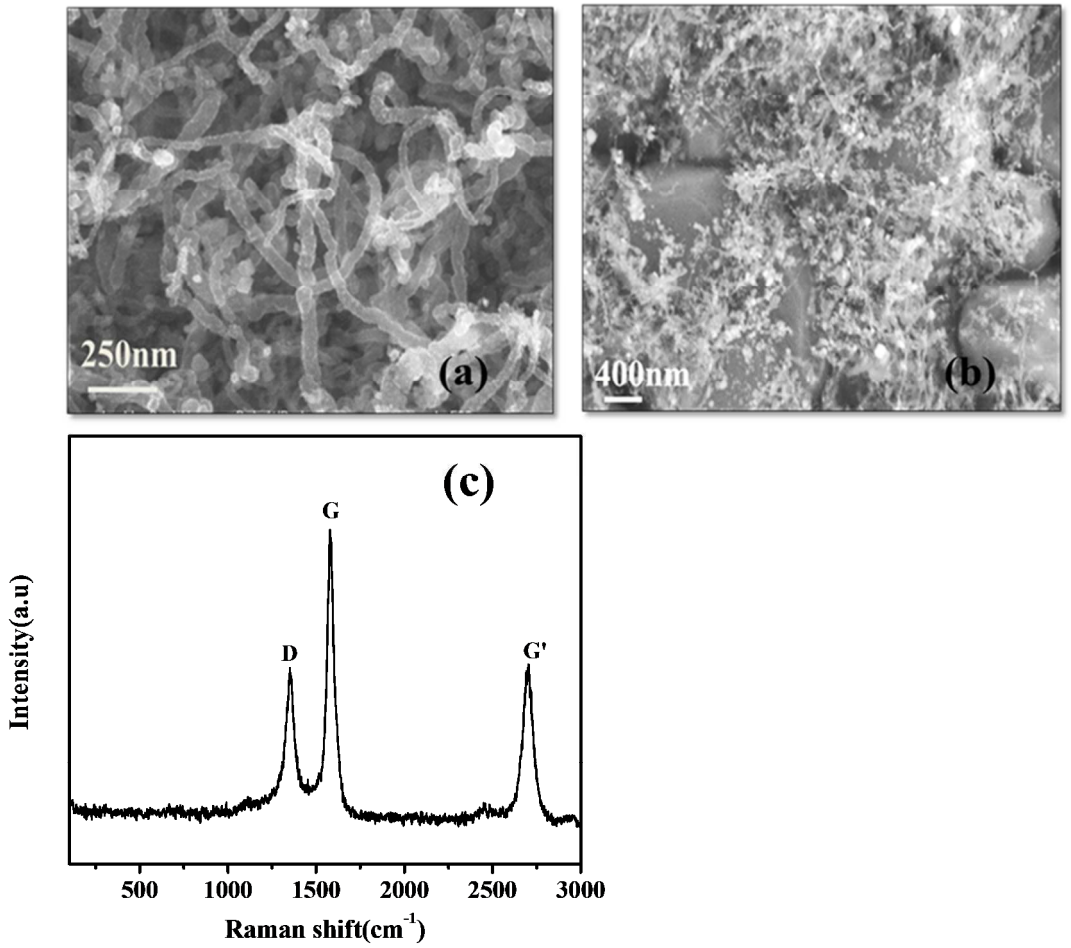

Fig. 11 SEM micrographs of the coating formed on (a) Si (b) Al_2O_3 at 30 torr, displaying CNT growth, with differing morphologies (c) Raman spectrum of the film formed on Si(100) at 700°C and 30 torr

The XPS spectrum of film on silicon also shows the presence of Fe and Fe_3O_4 (supplementary information). Although CNTs are deposited on Si (100), there is no evidence in the Raman spectrum for the deposition of iron oxide, indicating that a much smaller proportion of Fe_3O_4 is perhaps formed on silicon than in the film on SS316. This illustrates qualitatively the influence of the chemical nature of the substrate on the pathways of chemical reactions in the CVD process.

The results presented above prove that CNT formation is an intrinsic part of the inert-ambient CVD process with $Fe(acac)_3$ as the precursor, and that it is independent of the substrate used. The proportion of CNTs and Fe_3O_4 formed, the structural characteristics of CNT, and thus

the final morphology of the film, were found to be substrate-specific. For example, films obtained on silicon, SS316, and alumina, simultaneously, display different morphologies (Fig. 4(a), 11(a) and (b)).

Metal-organic route for composite formation

The results described above establish clearly that metal acetylacetonates in particular – and metal β-diketonates in general - can be used as single-source precursors for obtaining carbonaceous composites through inert-ambient CVD[24]. It has been generally believed that the formation of CNTs by CVD requires (or is facilitated by) the presence of fine particles of a transition metal to catalyse the high-temperature decomposition of a hydrocarbon or other carbon source. The formation of CNTs in the present process was unexpected – even remarkable - because the chemical source available was only $Fe(acac)_3$, a metalorganic complex in which Fe is bound to oxygen and carbon is bound to oxygen and hydrogen. A mechanism for the formation of such a composite may be formulated (as below) by considering results of the detailed characterization of the deposits carried out. The most significant feature of the depositions is the formation of finely divided elemental iron, which is ordinarily prone to rapid oxidation. The samples were analysed by XPS months after they were prepared, testifying to the stability of iron in it against oxidation. This stability is due to the "passivation" provided by the carbon that envelops the elemental iron – either CNTs enclosing it or amorphous carbon that surrounds it, evidenced by SEM and TEM analysis (Fig. 9).

The formation of elemental iron which, in turn, catalyses the formation of carbon nanotubes from the hydrocarbon moieties of the iron complex, may be explained as follows. At the elevated temperature and inert (highly reducing) ambient of the CVD chamber, the decomposition of the iron complex may be expected to lead to the formation of $Fe_{1-x}O$ (wuestite), Fe_3O_4 (magnetite), and iron carbide, Fe_3C, and elemental carbon[39]. Iron carbide is unstable in a carbon-rich environment at high temperatures, and decomposes into Fe and C[57-59]. The formation of Fe catalyses the formation of CNTs. The magnetite in the composite is likely to be formed during the cool-down from the deposition temperature, due to the disproportionation of $Fe_{1-x}O$ into Fe and Fe_3O_4 at temperatures <567°C [60]. Thus, the product is a composite of Fe, Fe_3O_4, and C, with the carbon "turned into" the CNT form under optimum CVD conditions[39].

Since the deposition involves the formation of Fe^0, the process becomes very sensitive to the presence of oxygen. Therefore, minute leaks in the CVD system can pose problems of

reproducibility. Furthermore, any CVD condition that influences the decomposition pathways of the precursor affects the composition of the deposit – specifically, the formation of CNTs - significantly. As the difference in the free energy of formation of different forms of carbon is smal, This is probably the reason why, in the present effort, the formation of CNTs is found to occur over a limited range of reactor pressures.

Finally, comments are in order concerning some measurements made on the composite CNT/Fe/Fe_3O_4 coatings. The presence of a substantial proportion of carbon in the composite leads to appreciable electrical conductivity in the composite (measured resistivity at 300 K is ~0.5 Ω-cm). This, in turn, renders the material suitable for application as an electrode material in supercapacitors. This aspect has indeed been examined by the authors, but preliminary results indicate a rather low specific capacitance of ~55 F/g. The composites are also magnetic, because of the presence of both Fe and Fe_3O_4. However, the saturation magnetization (emu/g) is not high because of the large proportion of carbon present. Despite the presence of CNTs, the mechanical properties of the composites are compromised by the porous morphology and the presence of a substantial proportion of graphite in addition to CNTs.

Conclusions

Low-pressure, inert-ambient CVD with $Fe(acac)_3$ as precursor results in a unique three-component composite of iron, iron oxide, and carbon. With $Fe(acac)_3$ as precursor, under appropriate conditions, MWCNTs are formed along with Fe_3O_4 – the first time (to our knowledge) that CNTs have been synthesized from a metal coordination complex (as opposed to hydrocarbons). Elemental iron, formed under the strongly reducing conditions of the inert gas ambient, apparently catalyzes the growth of CNTs. Indeed, some CNTs formed enclose iron particles within them. Formation of a composite coating of Fe/Fe_3O_4/C takes place, irrespective of the substrate used. In all the cases, the metallic iron formed is protected by the carbon that encloses it or surrounds it.

Acknowledgments

The authors acknowledge gratefully the Centre for Nano Science and Engineering (CeNSE) and the Advanced Facility for Microscopy and Microanalysis (AFMM) of the Indian Institute of Science, for supporting analyses by XPS, SEM, and TEM reported in this study. The work was supported by a grant under the NPMASS, Govt. of India.

References

1. E. T. Thostenson, Z. Ren and T.-W. Chou, *Composites Science and Technology*, 2001, **61**, 1899-1912.
2. J. S. Sakamoto and B. Dunn, *Journal of The Electrochemical Society*, 2002, **149**, A26-A30.
3. L. Yang, S. Cheng, Y. Ding, X. Zhu, Z. L. Wang and M. Liu, *Nano Letters*, 2011, **12**, 321-325.
4. M. Zhi, C. Xiang, J. Li, M. Li and N. Wu, *Nanoscale*, 2013, **5**, 72-88.
5. Q. Zhang, J.-Q. Huang, W.-Z. Qian, Y.-Y. Zhang and F. Wei, *Small*, 2013, **9**, 1237-1265.
6. S. Bose, T. Kuila, A. K. Mishra, R. Rajasekar, N. H. Kim and J. H. Lee, *Journal of Materials Chemistry*, 2012, **22**, 767-784.
7. K. Woan, G. Pyrgiotakis and W. Sigmund, *Advanced Materials*, 2009, **21**, 2233-2239.
8. M. Zhu and G. Diao, *Nanoscale*, 2011, **3**, 2748-2767.
9. V. Subramanian, H. Zhu and B. Wei, *Electrochemistry Communications*, 2006, **8**, 827-832.
10. M. F. L. De Volder, S. H. Tawfick, R. H. Baughman and A. J. Hart, *Science*, 2013, **339**, 535-539.
11. E. Flahaut, A. Peigney, C. Laurent, C. Marlière, F. Chastel and A. Rousset, *Acta Materialia*, 2000, **48**, 3803-3812.
12. Y. He, L. Huang, J.-S. Cai, X.-M. Zheng and S.-G. Sun, *Electrochimica Acta*, 2010, **55**, 1140-1144.
13. D.-W. Kim, K.-Y. Rhee and S.-J. Park, *Journal of Alloys and Compounds*, 2012, **530**, 6-10.
14. B. Gao, C. Peng, G. Z. Chen and G. Li Puma, *Applied Catalysis B: Environmental*, 2008, **85**, 17-23.
15. J. Li, S. Tang, L. Lu and H. C. Zeng, *Journal of the American Chemical Society*, 2007, **129**, 9401-9409.
16. H. Zhang, G. Cao, Z. Wang, Y. Yang, Z. Shi and Z. Gu, *Nano Letters*, 2008, **8**, 2664-2668.
17. S.-B. Ma, K.-Y. Ahn, E.-S. Lee, K.-H. Oh and K.-B. Kim, *Carbon*, 2007, **45**, 375-382.
18. Y. Zhang, M. Xu, F. Wang, X. Song, Y. Wang and S. Yang, *The Journal of Physical Chemistry C*, 2013, **117**, 12346-12351.
19. J.-S. Ye, H. F. Cui, X. Liu, T. M. Lim, W.-D. Zhang and F.-S. Sheu, *Small*, 2005, **1**, 560-565.
20. Y. Zhang, X. Sun, L. Pan, H. Li, Z. Sun, C. Sun and B. K. Tay, *Solid State Ionics*, 2009, **180**, 1525-1528.
21. P. H. Jampani, K. Kadakia, D. H. Hong, R. Epur, J. A. Poston, A. Manivannan and P. N. Kumta, *Journal of The Electrochemical Society*, 2013, **160**, A1118-A1127.
22. L. Marot, T. de los Arcos, A. M. Bünzli, C. Wäckerlin, R. Steiner, P. Oelhafen, E. Meyer, D. Mathys, P. Spätig and G. Covarel, *Surface and Coatings Technology*, 2012, **212**, 223-228.
23. A. Varade, A. S. Shivashankar, S. Dhar and S. Sampath, *US Patent*, 2013, **8343572 B2**.
24. A. Varade and S. A. Shivashankar, *Carbon*, 2011, **49**, 1401-1407.
25. L. Machala, J. Tuček and R. Zbořil, *Chemistry of Materials*, 2011, **23**, 3255-3272.

26. R. M. Cornell and U. Schwertmann, *The Iron Oxides: Structure, Properties, Reactions, Occurrences and Uses*, Wiley, 2003.
27. Z. Shao-Min, Z. Xing-Tang, G. He-Chun, Z. Bin, W. Zhi-Shen, D. Zu-Liang and W. Si-Xin, *Journal of Physics: Condensed Matter*, 2008, **20**, 075217.
28. S. Mathur, V. Sivakov, H. Shen, S. Barth, C. Cavelius, A. Nilsson and P. Kuhn, *Thin Solid Films*, 2006, **502**, 88-93.
29. J. Bachmann, Jing, M. Knez, S. Barth, H. Shen, S. Mathur, U. Gösele and K. Nielsch, *Journal of the American Chemical Society*, 2007, **129**, 9554-9555.
30. W. Jiang, Y. Zhou, Y. Zhang, S. Xuan and X. Gong, *Dalton Transactions*, 2012, **41**, 4594-4601.
31. T. Maruyama and Y. Shinyashiki, *Thin Solid Films*, 1998, **333**, 203-206.
32. S. Dhara, G. L. Malhotra, A. C. Rastogi and B. K. Das, *Thin Solid Films*, 1992, **209**, 116-121.
33. A. C. Rastogi, S. Dhara and B. K. Das, *Journal of The Electrochemical Society*, 1995, **142**, 3148-3156.
34. K. Kuribayashi and R. Ueyama, *Thin Solid Films*, 1997, **295**, 16-18.
35. C. N. R. Rao and A. Govindaraj, *Accounts of Chemical Research*, 2002, **35**, 998-1007.
36. R. Sen, A. Govindaraj and C. N. R. Rao, *Chemical Physics Letters*, 1997, **267**, 276-280.
37. N. S. Kim, Y. T. Lee, J. Park, J. B. Han, Y. S. Choi, S. Y. Choi, J. Choo and G. H. Lee, *The Journal of Physical Chemistry B*, 2003, **107**, 9249-9255.
38. J. Prasek, J. Drbohlavova, J. Chomoucka, J. Hubalek, O. Jasek, V. Adam and R. Kizek, *Journal of Materials Chemistry*, 2011, **21**, 15872-15884.
39. S. Dhar, P. Arod, K. V. L. V. Narayan Achari and S. A. Shivashankar, *MRS Online Proceedings Library*, 2015, **1752**, null-null.
40. X. Zhao, D. Xia and K. Zheng, *ACS Applied Materials & Interfaces*, 2012, **4**, 1350-1356.
41. Y. Li, Q. Meng, S.-m. Zhu, Z.-h. Sun, H. Yang, Z.-x. Chen, C.-l. Zhu, Z.-p. Guo and D. Zhang, *Dalton Transactions*, 2015, **44**, 4594-4600.
42. J. Li, Z. Ai and L. Zhang, *Journal of Hazardous Materials*, 2009, **164**, 18-25.
43. M. Busch, W. Schmidt, V. Migunov, A. Beckel, C. Notthoff, A. Kompch, U. Bergmann, M. Winterer and B. Atakan, *Applied Catalysis B: Environmental*, 2014, **160–161**, 641-650.
44. P. Bhunia, G. Kim, C. Baik and H. Lee, *Chemical Communications*, 2012, **48**, 9888-9890.
45. F. Tuinstra and J. L. Koenig, *The Journal of Chemical Physics*, 1970, **53**, 1126-1130.
46. A. C. Ferrari and J. Robertson, *Physical Review B*, 2000, **61**, 14095-14107.
47. P. K. Chu and L. Li, *Materials Chemistry and Physics*, 2006, **96**, 253-277.
48. R. Escribano, J. J. Sloan, N. Siddique, N. Sze and T. Dudev, *Vibrational Spectroscopy*, 2001, **26**, 179-186.
49. Y. Wang, D. C. Alsmeyer and R. L. McCreery, *Chemistry of Materials*, 1990, **2**, 557-563.
50. O. N. Shebanova and P. Lazor, *Journal of Solid State Chemistry*, 2003, **174**, 424-430.
51. A. M. Jubb and H. C. Allen, *ACS Applied Materials & Interfaces*, 2010, **2**, 2804-2812.
52. I. Chourpa, L. Douziech-Eyrolles, L. Ngaboni-Okassa, J.-F. Fouquenet, S. Cohen-Jonathan, M. Souce, H. Marchais and P. Dubois, *Analyst*, 2005, **130**, 1395-1403.
53. M. S. Dresselhaus, G. Dresselhaus, R. Saito and A. Jorio, *Physics Reports*, 2005, **409**, 47-99.

54. C. S. Kuivila, J. B. Butt and P. C. Stair, *Applied Surface Science*, 1988, **32**, 99-121.
55. N. S. McIntyre and D. G. Zetaruk, *Analytical Chemistry*, 1977, **49**, 1521-1529.
56. T.-C. Lin, G. Seshadri and J. A. Kelber, *Applied Surface Science*, 1997, **119**, 83-92.
57. A. Schneider, *Corrosion Science*, 2002, **44**, 2353-2365.
58. Q. Wei, E. Pippel, J. Woltersdorf and H. J. Grabke, *Materials and Corrosion*, 1999, **50**, 628-633.
59. C. Giordano, A. Kraupner, I. Fleischer, C. Henrich, G. Klingelhofer and M. Antonietti, *Journal of Materials Chemistry*, 2011, **21**, 16963-16967.
60. R. M. Cornell and U. Schwertmann, in *The Iron Oxides*, Wiley-VCH Verlag GmbH & Co. KGaA, 2004, DOI: 10.1002/3527602097.ch2, pp. 9-38.